Study of KrO^- and KrO via Slow Photoelectron Velocity-Map Imaging Spectroscopy and ab Initio Calculations†

Etienne Garand,‡ Alexei A. Buchachenko,*,§ Tara I. Yacovitch,‡ Małgorzata M. Szczęśniak,⊥ Grzegorz Chałasiński,⊥,|| and Daniel M. Neumark*,‡,#

Department of Chemistry, University of California—Berkeley, Berkeley, California 94720, Laboratory of Molecular Structure and Quantum Mechanics, Department of Chemistry, Moscow State University, Moscow 119991, Russia, Department of Chemistry, Oakland University, Rochester, Michigan 48309, Faculty of Chemistry, University of Warsaw, Pasteura 1, 02-093 Warszawa, Poland, and Chemical Sciences Division, Lawrence Berkeley National Laboratory, Berkeley, California, 94720

Received: April 25, 2009; Revised Manuscript Received: June 1, 2009

The high-resolution photoelectron spectrum of KrO^- was obtained using slow electron velocity-map imaging (SEVI). The SEVI spectrum reveals numerous vibronic transitions between multiple electronic states of KrO^- and KrO, both of which are open-shell species. Detailed assignments are made by comparison with theoretical simulations based on high level ab initio calculations and an atoms-in-molecule model that accounts for spin−orbit coupling in the anion and neutral. Several KrO^- and KrO vibrational frequencies and excited-state term energies are accurately determined from the analysis of the experimental spectra and are found to be in good agreement with the calculated values.

I. Introduction

Photoelectron (PE) spectroscopy of molecular anions is a versatile method for determining electron affinities, excited state term energies, and vibrational frequencies of the corresponding neutral species.[1] However, its limited energy resolution (5−10 meV) restricts the degree to which low-frequency vibrational modes can be resolved. This deficiency has been addressed using a related higher resolution technique, anion zero energy kinetic energy (ZEKE) spectroscopy,[2] which has been applied to the study of several weakly bound open-shell rare-gas halide complexes via photodetachment of the appropriate anion.[3−6] ZEKE spectroscopy resolves the closely spaced vibrational levels supported by these electronic states and thus yields spectroscopic information that is highly complementary to scattering experiments on the same systems.[7] Accurate experimental spectroscopic constants for the anion and neutral complexes can be extracted from the spectra and compared to ab initio calculated interaction potentials of these species. The recently developed slow electron velocity-map imaging (SEVI) technique, which is a hybrid between ZEKE and conventional PE spectroscopy, has been used to study the ClH_2 and ArO van der Waals complexes by photodetachment of ClH_2^- and ArO^-.[8,9] SEVI offers comparable resolution to anion ZEKE (2−3 cm^{-1}) but is considerably easier to implement.[10]

In this paper, we continue our investigation of rare-gas oxides using the SEVI technique by studying KrO^- and KrO. These species are both open shell complexes with $^2\Sigma^+$ and $^3\Pi$ ground states, respectively, and have several low-lying electronic states. Hence, the extraction of accurate potential energy curves for the anion and neutral poses a challenge for both experiment and theory.

Early studies on the rare gas oxides were motivated by their possible application in excimer lasers.[11−13] The first experimental data on the interaction potentials between rare-gas and oxygen atoms was obtained from the beam scattering experiments of Aquilanti and co-workers.[14−18] de Clercq et al. have studied KrO^- via conventional PE spectroscopy.[19] The resolution of their apparatus (∼200 cm^{-1}) did not allow the observation of individual vibronic transitions. However, a bimodal structure with temperature-dependent relative intensity was observed and attributed to transitions originating from the ground state and the two low-lying excited states of the anion.

On the theoretical side, an atoms-in-molecule model in conjunction with ab initio calculations has been implemented to construct potential energy curves for the anion and neutral electronic states, including spin−orbit (SO) coupling, and to evaluate the PE transition probabilities.[20] The KrO^- PE spectrum simulated using this approach was found to be in good agreement with the experimental measurements.[21] Unfortunately, as explained in ref 9, these simulations were affected by a programming error which led to the absence of many bound−bound transitions in the simulations, a defect that was not apparent by comparison with the broad envelopes of the measured low-resolution PE spectra.

In this paper, we present high-resolution photoelectron spectra of KrO^- obtained using SEVI. Numerous transitions are observed within the broad envelope of the previous low-resolution photoelectron spectra. The accompanying theoretical sections rely on the advanced description of the KrO^- and KrO, namely, the calculation of interaction potentials with the coupled cluster method and extended basis set and the ab initio analysis of the scalar relativistic effects and vectorial spin−orbit coupling. These curves are incorporated into a simulation procedure[9,20] that accounts correctly for all of the bound−bound transition intensities and, in addition, includes the contribution

† Part of the "Vincenzo Aquilanti Festschrift".

* Authors to whom correspondence should be addressed. E-mail: alexei@classic.chem.msu.su (A.A.B.); dneumark@berkeley.edu (D.M.N.).
‡ University of California, Berkeley.
§ Moscow State University.
⊥ Oakland University.
|| University of Warsaw.
Lawrence Berkeley National Laboratory.

10.1021/jp903819m
Published on Web 07/01/2009

of bound-free (dissociative photodetachment) transitions. Comparison of the simulated and experimental SEVI spectra facilitates assignment of the many resolved features. Several spectroscopic constants for KrO^- and KrO determined from analysis of the experimental spectra are found to agree with the calculated values.

II. Experimental Section

The SEVI apparatus has been described in detail elsewhere.[10,22] SEVI is a high resolution variant of PE spectroscopy in which mass-selected anions are photodetached at a series of wavelengths. The resulting photoelectrons are collected by velocity-map imaging (VMI)[23] using relatively low extraction voltages, with the goal of selectively detecting slow electrons with high efficiency and enlarging their image on the detector. At each wavelength, one obtains a high resolution photoelectron spectrum over a limited range of electron kinetic energy.

KrO^- anions were produced from a gas mixture comprising 0.1% N_2O and 10% krypton in a balance of neon. The gas mixture, at a stagnation pressure of 350 psi, was expanded into the source vacuum chamber through an Even-Lavie pulsed valve[24] equipped with a circular ionizer. The anions were then perpendicularly extracted into a Wiley−McLaren time-of-flight mass spectrometer[25] and directed to the detachment region by a series of electrostatic lenses and pinholes. A pulse on the last ion deflector allowed only the desired mass into the interaction region. Anions were photodetached between the repeller and the extraction plates of the VMI stack by the gently focused output of a Nd:YAG-pumped tunable dye laser. The photoelectron cloud formed was coaxially extracted down a 50 cm flight tube and mapped onto a detector comprising a chevron-mounted pair of time-gated, imaging quality microchannel plates coupled to a phosphor screen, as is typically used in photofragment imaging experiments.[26] Events on the screen were collected by a 1024 × 1024 charge-coupled device (CCD) camera and sent to a computer. Electron velocity-mapped images resulting from 30 000−50 000 laser pulses were summed, quadrant symmetrized, and inverse-Abel transformed. Photoelectron spectra were obtained via angular integration of the transformed images. The spectra presented here are plotted with respect to electron binding energy (eBE), defined as the difference between the energy of the photodetachment photon and the measured electron kinetic energy (eKE).

The apparatus was calibrated by acquiring SEVI images of atomic oxygen[27] at several different photon energies. In the SEVI experiment, within the same image, all observed transitions have similar widths in pixels (Δr), which means transitions observed further from threshold (larger r) are broader in energy. With the -200 V VMI repeller voltage used in this study, the full widths at half-maximum (fwhm) Γ of the oxygen peaks were 2.2 cm^{-1} at 20 cm^{-1} eKE and 6.8 cm^{-1} at 150 cm^{-1} eKE. The dependence of Γ upon eKE was found to fit a quadratic expression

$$\Gamma = 2.0 + 0.031(\text{eKE}) - 1.3 \times 10^{-5}(\text{eKE})^2 \qquad (1)$$

where all units are in wavenumbers.

III. Experimental Results

The SEVI spectrum of KrO^-, taken at a photon energy E_0 = 13334.6 cm^{-1}, is shown in Figure 1. The spectrum is quite congested, with most transitions occurring between 12 900 and 13 200 cm^{-1}. Clearly discernible peaks are labeled by capital letters A-P and their positions are listed in Table 1. The estimated error bars are ±5 cm^{-1}. There are at least two prominent progressions starting with peaks C and K, with characteristic peak spacings of 20−30 cm^{-1}. These progressions appear to lie above a smoothly varying background signal that peaks around 13025 cm^{-1}, but one cannot tell from the spectrum alone if this background results from spectral congestion or transitions to continuum states of the neutral complex. Weak structure is also observed below 12 900 cm^{-1}. The most prominent features here are peaks A and B at 12 610 and 12 640 cm^{-1}, respectively. Other features are labeled by small letters a-k. A detailed assignment of the SEVI peaks can be made by comparison with the theoretical results presented in section IV.

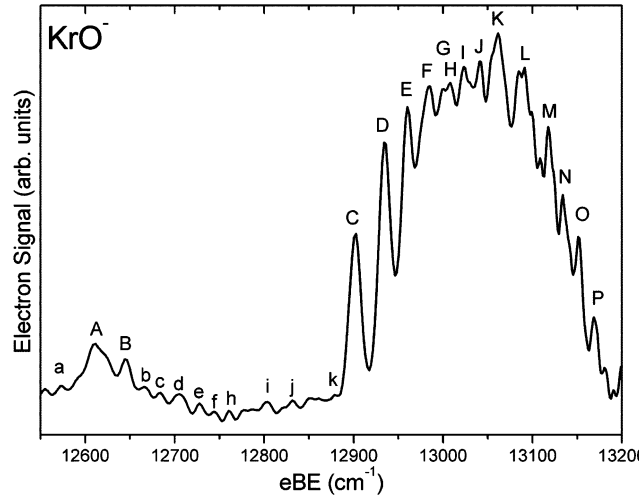

Figure 1. SEVI spectrum of KrO^- taken at 13334.6 cm^{-1} photon energy.

The transitions shown in Figure 1 occur within the two broad overlapping envelopes of the PE spectrum reported by de Clercq et al.[19] The region of maximum intensity in the SEVI spectrum approximately coincides with the peak of the "X" features in the PE spectrum near 13 100 cm^{-1}. However, compared to the PE spectrum, the SEVI spectrum displays much less intensity at eBE < 12 900 cm^{-1}. De Clercq et al. found that the feature "A" in this region was sensitive to ion source conditions and presumably resulted from "hot band" transitions originating from electronically excited anions. Peak A in the SEVI spectrum coincides with the maximum of the feature "A" near 12 600 cm^{-1} in the PE spectrum. Hence, the intensity differences between the SEVI and PE spectra suggest lower anion temperatures in the SEVI experiment, similar to what was observed for ArO^-.[9]

IV. Theory

A. Electronic Structure and Adiabatic Potentials. ***1. Ab Initio Potentials.*** The electronic structure of the RgO^- anions and RgO neutrals is described in detail elsewhere.[9,20] In brief, under the *LS* coupling scheme [appropriate for both nonrelativistic and scalar relativistic (SR) approximations], the interaction of Rg(^{1}S) and O(^{3}P) atoms gives rise to two terms of $^3\Sigma^-$ and $^3\Pi$ symmetry, whereas the interaction between Rg(^{1}S) and the O^-(^{2}P) anion gives two states of $^2\Sigma^+$ and $^2\Pi$ symmetry. Following the notation of the previous studies,[9,20,21] we will denote these potentials as V_{Σ}^{-}, V_{Π}, V_{Σ} and V_{Π}, respectively.

A set of these potentials was obtained previously[28] for the purpose of interpreting the lower-resolution KrO^- PE spectra.[19,21] The restricted version of the coupled cluster method with single, double and noniterative triple excitations, RCCSD(T), and the

TABLE 1: Experimental and Calculated Peaks Positions (cm^{-1}) and Shift from Origin along with Transition Assignments[a]

peak	exptl eBE	shift	theory eBE	shift	δ(exp-theory) (eBE)	δ(exp-theory) (shift)	assignment
a	12572	−330	12577.2	−314.7	−5	15	*II*1,0← *I*,3
A	12611	−291	12608.5	−283.4	2	8	*X*2,0← *I*,0
B	12644	−258	12640.3	−251.6	4	6	*X*2,1← *I*,0
b	12665	−237	12658.3	−233.6	7	3	*I*1,1← *I*,0
c	12684	−218	12675.8	−216.1	8	2	*I*1,2← *I*,0
d	12705	−197	12698.1	−193.4	7	4	*X*2,0←*X*,2
e	12728	−174	12725.0	−166.9	3	7	*I*1,0←*X*,2
f	12743	−159	12747.9	−144.0	5	15	*I*1,1←*X*,2
g	12760	−142	12765.3	−126.6	5	15	*I*1,2←*X*,2
h	12803	−99	12791.8	−100.1	11	−1	*X*2,0←*X*,1
i	12832	−70	12823.6	−68.3	8	2	*X*2,1←*X*,1
j	12852	−50	12847.7	−44.2	4	6	*X*2,2←*X*,1
k	12878	−24	12870.8	−21.1	9	3	*I*1,3←*X*,1
C	12902	0	12891.9	0	10	0	*X*2,0←*X*,0
D	12934	32	12923.7	31.8	10	0	*X*2,1←*X*,0
E	12960	58	12947.8	55.9	12	−2	*X*2,2←*X*,0
F	12984	82	12964.4	72.5	20	−10	*X*2,3←*X*,0
G	12999	97	12974.2	82.3	25	−15	*X*2,4←*X*,0
H*	13008	106	12978.7	86.9	29	−19	*X*2,5←*X*,0
I*	13023	121	13005.8	113.9	17	−7	*II*0,2←*X*,1
J*	13041	139	13022.4	130.5	19	−9	*II*0,3←*X*,1
K	13061	159	13049.9	158.1	11	−1	*II*0,0←*X*,0
L	13091	189	13081.8	189.9	9	1	*II*0,1←*X*,0
M	13118	216	13105.9	214.0	12	−2	*II*0,2←*X*,0
N	13134	232	13122.5	230.6	12	−1	*II*0,3←*X*,0
O	13151	249	13132.3	240.5	19	−9	*II*0,4←*X*,0
P*	13169	267	13136.8	245.0	32	−22	*II*0,5←*X*,0

[a] The features labeled a-k and those marked with and asterisk are tentatively assigned.

augmented correlation consistent aug-cc-pV*n*Z (AV*n*Z) $n = T$, Q basis sets[29−31] with the addition of the 3s3p2d set of bond functions (bf332) placed at the midpoint of internuclear distance *R* was implemented. However, experience with the SEVI spectroscopy of ArO^-[9] indicates that this level may not be high enough to reproduce the high-resolution spectra accurately. Thus, refined ab initio calculations have been performed as described below.

All calculations of the interaction energies implemented the RCCSD(T) method to correlate the electrons of the 2s2p shells of the O atom or anion and 4s4p or 3d4s4p shells of the Kr atom. Three types of approaches were used to assess the scalar relativistic effects. In the first approach, no relativistic correction was taken into account. These all-electron calculations were performed using AV5Z basis sets for both Kr and O centers. In the second, scalar relativistic effects were included using the second-order Douglas-Kroll-Hess Hamiltonian (DK) in combination with specially optimized AV5Z-DK basis set for O and AV5Z basis for Kr. Further extension of the basis set denoted as DAV5Z or DAV5Z-DK was achieved by using the doubly augmented V5Z set for O and adding one primitive in each of the spdfgh symmetry types with the exponent continuing the even-tempered sequence of the smallest two exponents of the standard AV5Z basis for Kr. The third approach used the ECP10MDF relativistic effective core potential[32] (ECP) for Kr and supplementary AV5Z-PP and DAV5Z-PP basis sets. In some cases, the 3s3p2d2f1g bond function set (bf)[33] was placed at the midpoint of internuclear distance. Interaction energies were computed over a tight grid in *R* from 1.8 to 25 Å and corrected for basis set superposition error using the full counterpoise correction scheme.[34] All calculations were performed with the MOLPRO program package.[35]

Equilibrium distances and interaction energies for the ab initio potentials computed as described above are presented in Table 2 along with some previous data. It can be seen that both correlation of Kr(3d) shell and inclusion of the SR effects are important. The former was therefore included in almost all calculations. At the AV5Z level, SR effects in the KrO neutral make both the $^3\Sigma^-$ and $^3\Pi$ interaction potentials deeper, to a very similar extent for DK and ECP calculations. For the KrO^- anion, DK and ECP calculations give qualitatively different results: their effects are opposite for the binding energy of the $^2\Sigma^+$ state and quite different in magnitude for the $^2\Pi$ state. Extension of the basis set to DAV5Z level decreases the equilibrium distance and increases the binding energy for all the potentials to the degree almost identical in both DK and ECP calculations. Inclusion of the bond functions leads to the same effects, again very similar for KrO^-, but significantly larger in the DK than in the ECP calculations for KrO. Overall, bond functions produce stronger effects than inclusion of the extra diffuse primitives to the atomic basis. Unfortunately, all-electron DAV5Z+bf calculations were found to be too demanding.

The results presented in the Table 2 indicate good convergence with respect to the basis set extension. As is typical for weakly bound systems, saturation of the basis set pushes down the binding energy and contracts the bond length. Previous results[21,28] obtained with smaller basis sets are in line with the present calculations. In what follows, we will use the best DAV5Z-PP+bf SR potentials.

To assess the accuracy of the calculations and analyze the long-range (LR) behavior of the potentials, static atomic polarizabilities were computed by the finite-field method using the same level of theory. The dipole polarizability of Kr was estimated as 16.77, 16.67, and 16.78 a_0^3 for DAV5Z-DK and DAV5Z-PP calculations, respectively, in good agreement with the recommended value[36] of 16.76 a_0^3. Quadrupole polarizabilities of 92.9, 91.0, and 95.2 a_0^5 calculated for the same sequence, also agree well with the value 97.1 a_0^5 presented by Koutselos et al.[37] Dipole polarizabilities of the oxygen atom are practically independent of the DK correction and were estimated, using

TABLE 2: Equilibrium Distances R_e (Å) and Binding Energies D_e (cm^{-1}) Calculated for the KrO and KrO^- Systems by the RCCSD(T) Method Using Different Basis Set and Scalar Relativistic Corrections

	$KrO(^3\Pi)$		$KrO(^3\Sigma^-)$		$KrO^-(^2\Sigma^+)$		$KrO^-(^2\Pi)$	
basis set	R_e	D_e	R_e	D_e	R_e	D_e	R_e	D_e
AV5Z[a]	3.470	98.3	3.951	53.2	3.007	1189.2	3.356	864.0
AV5Z	3.465	99.1	3.945	53.6	2.967	1267.0	3.324	911.3
AV5Z-DK	3.456	100.0	3.946	54.3	2.964	1264.5	3.315	921.8
AV5Z-PP	3.455	100.1	3.946	54.4	2.959	1278.0	3.306	938.5
DAV5Z-DK	3.448	104.4	3.931	56.9	2.962	1275.9	3.313	931.3
DAV5Z-PP	3.445	104.6	3.933	57.0	2.957	1289.1	3.301	947.8
AV5Z-DK+bf	3.448	109.1	3.913	59.4	2.958	1281.6	3.311	936.7
AV5Z-PP+bf	3.449	106.7	3.925	58.2	2.951	1295.8	3.293	952.7
DAV5Z-PP+bf	3.448	107.0	3.925	58.3	2.951	1296.4	3.293	953.0
AVTZ+bf332[a,b]	3.467	103.5	3.956	55.0	2.963	1277.8	3.322	922.9
Scattering[c]	3.57 ± 0.07	105.7 ± 10.6	4.05 ± 0.08	45.2 ± 4.5				

[a] Kr(3d) shell is not correlated. [b] From refs 21 and 28. [c] From ref 18.

the DAV5Z basis set, as 5.83 and 4.94 a_0^3 for the $\Lambda = 0$ and $\Lambda = 1$ components, respectively. The isotropic $\alpha_0 = 5.24$ a_0^3 polarizability agrees well with the measured value[38] of 5.2 ± 0.4 a_0^3 and numerous theoretical estimates.[36,39,40] The anisotropic polarizability $\alpha_2 = -0.30$ a_0^3 is slightly less than the value of -0.36 a_0^3 computed by Medved et al.[40] using the second-order complete active space perturbation theory (CASPT2). For O^-, we found 20.63 and 39.98 a_0^3 for the $\Lambda = 0$ and $\Lambda = 1$ components, respectively, or 33.55 and 6.43 a_0^3 for isotropic and anisotropic polarizabilities. Post Hartree−Fock calculations by Mukherjee and co-workers[41] give α_0 ranging from 26.5 to 40.8 and α_2 from 4.6 to 8.1 a_0^3, in agreement with the more accurate present data. In contrast, ref 40 reports unexpectedly small values of 17.40 and 2.14 a_0^3 for isotropic and anisotropic polarizabilities, respectively.

The most accurate DAV5Z-PP+bf interaction potentials were fitted to an asymptotic LR expansion. For KrO, the dispersion coefficients C_6 and C_8 were found to be 46.8 and 1825 au for the $^3\Sigma^-$ state and 44.1 and 1250 au for the $^3\Pi$ state. Conversion of the lowest-order coefficient to the anisotropic representation[16] gives $C_{6,0} = 45.0$ au and $C_{6,2} = 4.5$ au Aquilanti and co-workers[18] used $C_{6,0} = 64.8$ au as estimated from the average velocity dependence of the scattering cross section. Overestimation is expected in this analysis because no higher-order terms were taken into account. For KrO^-, dispersion coefficients were determined after extraction of the lowest-order induction components proportional to R^{-4} and R^{-6} using the ab initio values of the dipole and quadrupole polarizabilities, respectively. The C_6 coefficients for the $^2\Sigma^+$ and $^2\Pi$ states are 29 and 192 au, respectively.

Additional hints on the accuracy of the KrO ab initio interaction potentials can be obtained by comparison to the beam scattering experiment by Aquilanti and co-workers.[18] The potentials derived from the measured absolute total scattering cross sections Q are characterized in Table 2. For the purpose of comparison, we performed the calculations of Q values for both ab initio and empirical scattering potentials using the same approach as implemented in ref 18. The cross sections were calculated for each adiabatic SO-coupled potential (see next subsection) as functions of collision velocity v and then summed according to the population of each atomic oxygen sublevel in the beam. Experimentally, these populations can be varied using a magnetic selector and ref 18 provides the data for zero and high magnetic fields that allow discrimination of the interaction anisotropy.

The results of the quantum calculations converged within 0.5% are plotted in Figure 2 using coordinates that emphasize

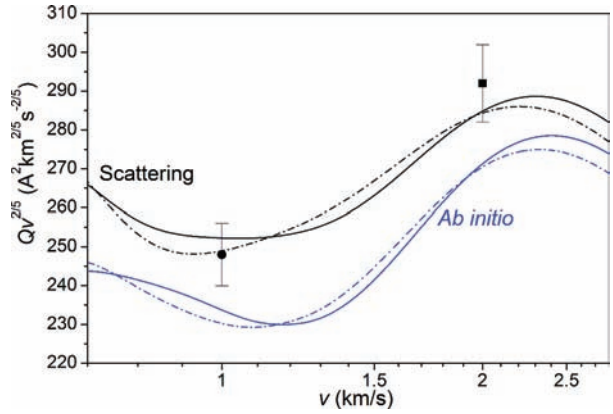

Figure 2. Velocity dependence of the absolute total scattering cross sections computed with ab initio and scattering potentials at zero (solid lines) and high (dot-dashed lines) magnetic field selection. Dot and square with error bars represent the measurements (from ref 18) at zero and high fields, respectively.

the glory scattering structure. The upper (lower) pair of curves represents the velocity dependence of the cross sections computed with scattering (ab initio) potentials at zero and high fields, whereas the symbols with error bars roughly indicate the measured data, as extracted from Figure 4 in ref 18. The ab initio potentials perfectly reproduce the glory pattern and magnetic field dependence, but systematically underestimate the absolute cross section values by 5.5%. It can be concluded that, at the level of the beam scattering sensitivity, ab initio calculations reproduce the shape and anisotropy of the KrO interaction, but underestimate its range. Indeed, Table 2 reveals a systematic underestimation of the equilibrium distances with respect to scattering potentials (note that within the hard-sphere approximation, the cross section value scales as a square of R_e).

2. SO-Coupled Potentials. The vectorial spin−orbit interaction splits atomic multiplets. The asymptotic energies Δ_j of the $Rg + O(^3P_j)$ limits counted from the lowest $j = 2$ term are $\Delta_1 = 158.27$ and $\Delta_0 = 226.98$ cm^{-1}.[42] At finite distances, there are six SO-coupled states *X*2(2), *I*1(2), *I*0(2), *II*1(1), *II*0(1), and *III*0(0) classified as $n\Omega(j)$, where n indexes the states with the same projection of the total electronic angular momentum j on the molecular axis Ω. The $Rg + O^-(^2P_{1/2})$ limit lies $\Delta^- = 177.14$ cm^{-1} above the ground $Rg + O^-(^2P_{3/2})$ limit.[27] Three states of the anion complex can be classified using similar $n^-\Omega^-(j^-)$ notations as *X*1/2(3/2), *I*3/2(3/2), and *II*1/2(1/2). The lowest anion $j^- = 3/2$ and neutral $j = 2$ limits are separated in energy by the electron affinity of atomic oxygen, $EA = 11784.7$ cm^{-1}.[27]

In previous work,[9,20,21] the vectorial SO interaction that couple Σ and Π states in both neutral and anion oxygen complexes

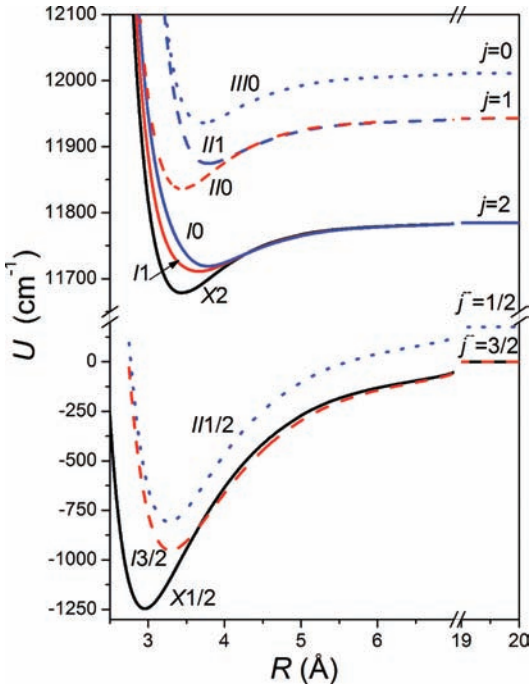

Figure 3. SO-coupled potentials of the anion and neutral KrO calculated using the atoms-in-molecule model and ab initio RCCSD(T)/DAV5Z-PP+bf SR potentials.

was taken into account within the so-called atoms-in-molecule model in which the coupling matrix elements are approximated by their atomic values. For the specific case of the ^2P or ^3P atoms interacting with rare gases, such models were considered in many studies (see, e.g., refs 3, 16, and 43 and references therein). According to this model, the SO-coupled potentials can are expressed analytically through four SR potentials $V_{\bar{\Sigma}}$, $V_{\bar{\Pi}}$, V_{Σ}, and V_{Π} and three atomic fine-structure energies Δ_1, Δ_0, and Δ^-.

To check the validity of this approximation, ab initio calculations of the SO-coupling matrix elements were performed. If the interactions of the states correlating to the ^2P or ^3P atomic multiplets with the higher-lying electronic states are neglected, the only nonzero matrix element of the SO operator V_{SO} in the former case is $\langle^2\Sigma^+|V_{SO}|^2\Pi\rangle = a^-(R)$, whereas in the latter case two matrix elements do not vanish, $\langle^3\Sigma^-|V_{SO}|^3\Pi\rangle/\sqrt{2} = \langle^3\Pi|V_{SO}|^3\Pi\rangle = a(R)$. The asymptotic splittings are related to these matrix elements by $\Delta^- = 3a^-$ and $\Delta_1 = 2a$, $\Delta_0 = 3a$. These relations imply that $\Delta_1/\Delta_0 = 2/3$ for oxygen atom. The experimental ratio[27] of 0.7 indicates that the ground state multiplet of the atom can indeed be considered as isolated.

The above matrix elements were computed using the complete active space multiconfigurational self-consistent field (CASSCF) method followed by state-interacting relativistic configuration interaction calculations with the full Breit-Pauli V_{SO} operator in the CASSCF internal space.[44] Asymptotically, these calculations gave $\Delta^- = 178.4$, $\Delta_1 = 154.8$, and $\Delta_0 = 232.3$ cm^{-1}, energies that agree with the measured term values within 3%. The matrix elements a^- and a weakly depend on internuclear distance. Their deviations from asymptotic values become significant only at distances that correspond to the high-energy repulsive branch of the SR potentials. The analysis of the SO-coupled potentials did not reveal any remarkable effect of these variations so we decided to use the atoms-in-molecule model with the asymptotic atomic parameters.

The SO-coupled potentials based on the most accurate DAV5Z-PP+bf SR potentials are depicted in Figure 3 and characterized in Table 3. Adiabatic transition energies T_0, dissociation energies D_0, and vibrational constants shown therein were obtained by solving the radial Schrödinger equations by the Numerov method for zero rotational angular momentum and fitting the lowest vibrational levels to the Dunham expansion. For the anion potentials, the 10 lowest levels were used, while all bound levels were used for the neutral potentials. T_0 values were calculated with respect to the ground vibronic level of the anion using the measured electron affinity of the oxygen atom.[27]

TABLE 3: Parameters of the SO-Coupled Potentials of the KrO Anion and Neutral Calculated Using the DAV5Z-PP+bf ab Initio Potentials

state	R_e (Å)	D_e (cm^{-1})	T_0 (cm^{-1})	D_0 (cm^{-1})	ω_e (cm^{-1})	$\omega_e x_e$ (cm^{-1})
			KrO^-			
*X*1/2	2.960	1247.8	0	1195.3	103.3	2.61
*I*3/2	3.293	953.0	283.4	911.9	82.5	2.05
*II*1/2	3.274	986.2	430.9	941.5	89.7	2.40
			KrO			
*X*2	3.448	107.0	0[a]	88.0	39.0	3.68
*I*1	3.652	74.1	26.9	61.0	28.4	2.76
*I*0	3.773	66.4	34.7	53.3	27.3	2.88
*II*1	3.768	69.1	192.2	53.8	29.8	3.34
*II*0	3.448	107.0	158.3	88.0	39.0	3.68
*III*0	3.699	76.1	254.9	59.7	33.1	3.90

[a] The calculated KrO electron affinity is 12 891.9 cm^{-1}.

B. Spectral Simulations. The SO-coupled potentials based on the RCCSD(T)/DAV5Z-PP+bf calculations were used for the spectral simulations. Details of the underlying theory have been presented elsewhere.[9,20] In brief, the simulations accounted for the bound−bound $n\Omega$, $v \leftarrow n^-$, v^- and bound-free $n\Omega$, $\varepsilon \leftarrow n^-$, v^- transitions, where v^- and v denote the vibrational levels in the particular electronic states of the anion n^- and neutral n, respectively, and ε specifies the kinetic energy of the Kr + O(^3P_j) products above the corresponding dissociation threshold. Rotational structure was not explicitly considered in the simulations. Solution of the radial Schrödinger equation provided anion and neutral vibronic energies E_{n-v-}, $E_{n\Omega v}$ and the corresponding wave functions that were used to calculate the vibronic line strength factors $I^{bb}(n\Omega,v \leftarrow n^- v^-)$ and $I^{bf}(n\Omega,\varepsilon \leftarrow n^- v^-)$ for the bound−bound and bound-free transitions, respectively. Introducing the initial population of the anion levels g_{n-v-} and the line shape function Θ, we expressed the full spectral envelope as

$$S(E) \propto \sum_{n^-}\sum_{v^-} g_{n^-v^-} \sum_{n\Omega} [\sum_{v} I^{bb}(n\Omega, v \leftarrow n^-v^-) \times \Theta(E - E_{n\Omega v} + E_{n^-v^-}) + \int_{-\infty}^{E_0} I^{bf}(n\Omega, E' \leftarrow n^-v^-) \times \Theta(E - E' + E_{n^-v^-})dE'] \quad (2)$$

The Θ function was assumed to have the Gaussian form with the width (fwhm) Γ multiplied by the factor $\sqrt{E_0 - E}$ in order to account for the threshold law for *s*-wave electron detachment at the fixed photon energy E_0.

V. Analysis and Discussion

A. Assignment. To assign the measured SEVI spectrum, preliminary simulations were performed with the set of the bound−bound transitions originating from the lowest 14 vibrational levels of anion in each electronic state and terminating

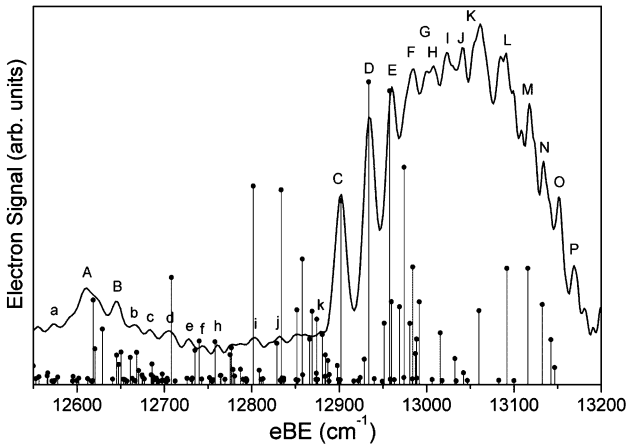

Figure 4. Experimental (solid line) and simulated (sticks) KrO^- SEVI spectrum including only the bound−bound transitions and assuming a 100 K equilibrium Boltzmann population of the anion levels. Simulated spectrum is shifted by 10 cm^{-1} toward higher eBE to match the position of the origin (peak C).

at all bound vibronic levels of the neutral. We explored temperatures in the range of $T = 20-100$ K to vary the population of the anion levels and used $\Gamma = 5-8$ cm^{-1} for the peak widths in eq 2. The bound−bound simulated stick spectrum calculated at $T = 100$K is shown in Figure 4. While these simulations provided only rough agreement with the experimental spectrum envelope, they allowed us to assign many prominent peaks in Figure 1 as indicated in Table 1. Most peaks at or above the eBE of peak C as well as peaks A and B could be readily assigned based on comparison with these simulations. The assignments of peaks H, I, and J, marked by asterisks in Table 1, are more tentative as they occur in the most congested region of the spectrum. Many of the smaller peaks (a-k) could also be assigned through comparison with these simulations or the more complete simulations discussed in the following section. For each peak, Table 1 gives the assignment, the absolute electron binding energy eBE, and the shifts with respect to the observed and calculated $X2$, $0 \leftarrow X$, 0 origin transitions. Table 1 also shows the differences, ΔeBE and ΔShift, between the observed and computed eBE and shift values, respectively.

Peaks labeled C−H are assigned to the $X2$, $v \leftarrow X$, 0 transitions where $v = 0-5$, respectively. Similarly, peaks K−P are assigned to the $II0$, $v \leftarrow X$, 0 transitions where $v = 0-5$. The predominance of transitions from the anion ground state to the various vibrational levels of the $X2$ and $II0$ neutral states is similar to what was observed in the SEVI spectrum of ArO−.[9] This result reflects the selectivity of the spin−orbit transitions but also the fact that these two states have an equilibrium geometry more similar to the anion ground state than the equilibrium geometries of the other neutral states.

The positions of the assigned features allow us to extract several experimental spectroscopic parameters, which can be compared with the calculations presented herein. The position of peak C gives the adiabatic electron affinity of 12902 ± 5 cm^{-1} (1.5996 ± 0.0006 eV) for KrO, which is very close to the calculated value of 12891.9 cm^{-1}. The relative positions of peaks C−H yield $\omega_e = 38.4 \pm 1$ cm^{-1} and $\omega_e x_e = 2.8 \pm 0.2$ cm^{-1} for the neutral $X2$ state. Similarly, peaks K−P yield $\omega_e = 35.5 \pm 2$ cm^{-1} and $\omega_e x_e = 2.6 \pm 0.5$ cm^{-1} for the $II0$ state. These two sets of values agree, within error bars, reflecting the fact that the neutral $X2$ and $II0$ curves should be identical (and the same as the KrO $^3\Pi$ state in Table 2). Moreover, the spacing between peaks C and K yields a term energy of 159 ± 5 cm^{-1} for the $II0$ state. This is consistent with the atom-in-molecule model in which the $X2$ and $II0$ curves are separated by the spin−orbit splitting ($\Delta_1 = 158.27$ cm^{-1}) of the oxygen atom.

By assuming that the $X2$ and $II0$ curves only support the 6 vibrational levels observed in the experimental spectra, the well depths of these two states can be determined to be $D_0 = 110 \pm 5$ and $D_0 = 113 \pm 5$ cm^{-1}. These values suggest that the calculations underestimate the well depth of the $X2$ and $II0$ potential curves by around 20 cm^{-1} and overestimate their anharmonicity. This discrepancy can be directly traced back to the V_Π potential because the $X2$ and $II0$ curves depend only on this potential in the spin−orbit model used here. By using the experimentally determined EA and D_0 of the $X2$ state, we can also determine the well depth of the X anion states to be $D_0 = 1225 \pm 10$ cm^{-1}, which is ∼30 cm^{-1} deeper than the calculated value.

Most of the other observed peaks can be assigned to "hot band" transitions originating from excited vibrational and/or electronic anion states. The most predominant of these features are peaks A and B which can be unambiguously assigned to the $X2$, $0 \leftarrow I$, 0 and $X2$, $1 \leftarrow I$, 0 transitions, respectively. This assignment allows us to determine the term energy of the anion I state to be $T_0 = 291 \pm 5$ cm^{-1} which is in good agreement with the 283.4 cm^{-1} calculated value. The remaining weaker peaks a-k and I,J are tentatively assigned to various hot band transitions mainly originating from the first two excited vibrational levels of the X anion state, based on the simulation and calculated positions.

B. Simulations. While simulations of the bound−bound transitions allowed us to assign peaks in the SEVI spectrum, they provided only a rough sketch of the measured spectral envelope. In attempt to reach better agreement, a more detailed analysis was undertaken.

A second set of simulations was carried out including the bound-free transitions as described in section IV.B. Also, it was found that the observed SEVI spectrum could not be fit well assuming a single-temperature Boltzmann distribution. We took into account only four low-lying initial states of the anion, namely $n^- = X$, $v^- = 0-2$ and $n^- = I$, $v^- = 0$, which, according to Table 1, are responsible for all observed features (except the weak peak a with the smallest eBE). Based on the transition probability ratios for individual transitions, as well as of the bound−bound simulations, the populations of the three excited states were set to 0.02 of the ground state population. All transitions from these states were included in the simulations. In order to remove the uncertainty in the line width parameter, the experimental peak width dependence (eq 1) was used to evaluate line shape function Θ in eq 2.

The simulated spectrum is compared with experiment in the Figure 5. It reproduces much of the structure below 13000 cm^{-1} associated with $X2$, $v \leftarrow X$, 0 transitions from the vibrational ground state, hot-band transitions at lower eBE, and transitions from the excited anion state at the low energy edge of the spectrum. However, above 13000 cm^{-1} (almost the threshold for dissociative detachment through the $X2 \leftarrow X$, 0 transition), significant disagreement is evident. The simulation does not reproduce the feature due to $X2$, $5 \leftarrow X$, 0 and $II2$, $5 \leftarrow X$, 0 transitions (peak H and P) because the final level is not supported by the too shallow ab initio potential. Underestimation of the total intensity and distortion of the pattern associated to the $II0$, $v \leftarrow X$, 0 progression reflects the bound-free contribution shown in Figure 5 separately as the shaded region. The bound-free continuous background appears too small and too diffuse.

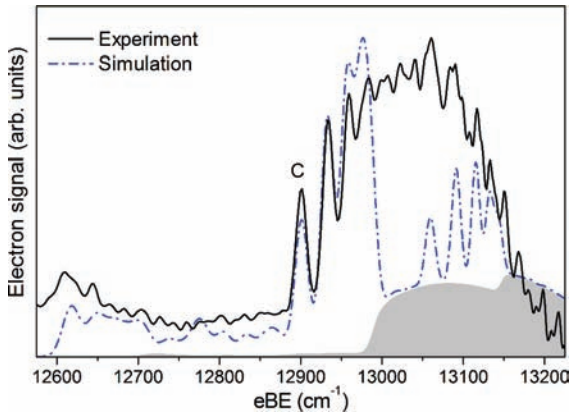

Figure 5. Experimental (solid line) and simulated (dashed line) KrO^- SEVI spectrum. Simulated spectrum is shifted by 10 cm^{-1} toward higher eBE to match the position of the origin (peak C). Shadowed region represents the bound-free transition contribution to the simulated envelope.

It develops too slowly at the threshold and decays too slowly at higher eBE.

Such behavior was found to be persistent. Neither scaling the depth of ab initio interaction potentials and shifting of their equilibrium distances, nor replacing the neutral potentials by the empirical scattering potentials from ref 18 improves the situation noticeably. Likewise, rotationally resolved simulations that used rotational line strength factors[3,20] failed to produce better agreement with the measurements in the region above 13000 cm^{-1}. These efforts suggest that the discrepancies between the measured and simulated spectra mostly originate from the photodetachment transition probability calculations. The model proposed in ref 20 and used here assumes that the rare-gas atom weakly interacts with the O− anion and that the ejected photoelectron interacts only with the oxygen atom. Indeed, this assumption is less valid for the relatively heavy and strongly polarizable Kr atom. The qualitatively similar discrepancies which appeared to be less pronounced in the ArO^- SEVI spectra[9] tends to support this explanation.

Finally, it is worthwhile to comment on the lower-resolution PE study by Bowen and co-workers.[19] As explained in ref.,[9] previous theoretical calculations[21] were subject to inaccuracies in the interaction potentials and to an error in the transition intensity evaluation. The full set of photodetachment transitions used above to assign the SEVI spectrum provides a good representation of the PE spectrum of KrO^- as well (not shown). In particular, one can reproduce the temperature evolution of the relative intensity of two broad peaks, one at eBE ca. 12 600 cm^{-1}, the other at 13 100 cm^{-1}. The latter peak corresponds to a feature dominating the SEVI spectrum, but with the structure completely washed out at the resolution of 200 cm^{-1}. The eBE of the peak is close to that of the SEVI peak A and is composed predominantly of transitions from the electronically excited *I* state and vibrationally excited levels of the anion *X*-state. The intensity of the low-eBE peak rises with temperature due to thermal excitations. Therefore, the situation is very close to that discussed for ArO^- anion[9] and corroborates the previous interpretation.[19,21]

VI. Conclusion

(1) The high resolution photoelectron spectrum of the KrO^- anion was obtained using slow electron velocity-map imaging. This technique provides enough resolution to discern rich vibronic structure hidden in the broad maxima of the previous conventional PE spectrum.[19] The SEVI spectrum of KrO^- resembles that of ArO^- reported previously, but is more congested and reveals more structure due to a higher density of states for the neutral product.

(2) Careful ab initio studies of KrO^- and KrO were carried out stressing the basis set quality, scalar relativistic and core correlation effects, and vectorial spin−orbit coupling.

(3) The spectral simulations that use the new ab initio potentials provide a detailed assignment of the measured spectrum in terms of vibronic transitions. This assignment is used to extract from the measured spectrum transition energies, dissociation energies and vibrational constants for the ground and some low-lying states of the anion and neutral systems.

(4) Comparison with experimental spectroscopic constants, as well as the assessment against the beam scattering data,[18] reveals that the ab initio potentials are not as accurate as expected taking into account the high level of the calculations and the depth of their theoretical assessment.

(5) Ab initio simulations fit the SEVI spectral envelope quite well, except for the region dominated by dissociative photodetachment.

Acknowledgment. This work was supported by the Air Force Office of Scientific Research under Grant No. FA9550-09-1-0343(DMN), the National Science Foundation under Grant No. CHE-0719260 (MMS and GC), and the Russian Basic Research Fund under Project No. 08-03-00414 (AAB). EG thanks the National Science and Engineering Research Council of Canada (NSERC) for a post graduate scholarship and TY thanks the Fonds Québécois de la Recherche sur la Nature et les Technologies (FQRNT) for a master's scholarship.

References and Notes

(1) Rienstra-Kiracofe, J. C.; Tschumper, G. S.; Schaefer, H. F.; Nandi, S.; Ellison, G. B. *Chem. Rev.* **2002**, *102*, 231.
(2) Kitsopoulos, T. N.; Waller, I. M.; Loeser, J. G.; Neumark, D. M. *Chem. Phys. Lett.* **1989**, *159*, 300.
(3) Zhao, Y. X.; Yourshaw, I.; Reiser, G.; Arnold, C. C.; Neumark, D. M. *J. Chem. Phys.* **1994**, *101*, 6538.
(4) Yourshaw, I.; Lenzer, T.; Reiser, G.; Neumark, D. M. *J. Chem. Phys.* **1998**, *109*, 5247.
(5) Lenzer, T.; Yourshaw, I.; Furlanetto, M. R.; Reiser, G.; Neumark, D. M. *J. Chem. Phys.* **1999**, *110*, 9578.
(6) Lenzer, T.; Yourshaw, I.; Furlanetto, M. R.; Pivonka, N. L.; Neumark, D. M. *J. Chem. Phys.* **2002**, *116*, 4170.
(7) Aquilanti, V.; Cappelletti, D.; Lorent, V.; Luzzatti, E.; Pirani, F. *J. Phys. Chem.* **1993**, *97*, 2063.
(8) Garand, E.; Zhou, J.; Manolopoulos, D. E.; Alexander, M. H.; Neumark, D. M. *Science* **2008**, *319*, 72.
(9) Garand, E.; Buchachenko, A. A.; Yacovitch, T. I.; Szczęśniak, M. M.; Chałasiński, G.; Neumark, D. M. *J. Phys. Chem. A* **2009**, *113*, 4631.
(10) Neumark, D. M. *J. Phys. Chem. A* **2008**, *112*, 13287.
(11) Powell, H. T.; Murray, J. R.; Rhodes, C. K. *Appl. Phys. Lett.* **1974**, *25*, 730.
(12) Dunning, T. H.; Hay, P. J. *J. Chem. Phys.* **1977**, *66*, 3767.
(13) Langhoff, S. R. *J. Chem. Phys.* **1980**, *73*, 2379.
(14) Aquilanti, V.; Liuti, G.; Pirani, F.; Vecchiocattivi, F.; Volpi, G. G. *J. Chem. Phys.* **1976**, *65*, 4751.
(15) Aquilanti, V.; Casavecchia, P.; Grossi, G.; Lagana, A. *J. Chem. Phys.* **1980**, *73*, 1173.
(16) Aquilanti, V.; Grossi, G. *J. Chem. Phys.* **1980**, *73*, 1165.
(17) Aquilanti, V.; Luzzatti, E.; Pirani, F.; Volpi, G. G. *J. Chem. Phys.* **1980**, *73*, 1181.
(18) Aquilanti, V.; Candori, R.; Pirani, F. *J. Chem. Phys.* **1988**, *89*, 6157.
(19) de Clercq, H. L.; Hendricks, J. H.; Bowen, K. H. *J. Chem. Phys.* **2002**, *117*, 2619.
(20) Buchachenko, A. A.; Jakowski, J.; Chalasinski, G.; Szczesniak, M. M.; Cybulski, S. M. *J. Chem. Phys.* **2000**, *112*, 5852.
(21) Buchachenko, A. A.; Szczesniak, M. M.; Klos, J.; Chalasinski, G. *J. Chem. Phys.* **2002**, *117*, 2629.
(22) Osterwalder, A.; Nee, M. J.; Zhou, J.; Neumark, D. M. *J. Chem. Phys.* **2004**, *121*, 6317.
(23) Eppink, A.; Parker, D. H. *Rev. Sci. Instrum.* **1997**, *68*, 3477.

(24) Even, U.; Jortner, J.; Noy, D.; Lavie, N.; Cossart-Magos, C. *J. Chem. Phys.* **2000**, *112*, 8068.
(25) Wiley, W. C.; McLaren, I. H. *Rev. Sci. Instrum.* **1955**, *26*, 1150.
(26) Chandler, D. W.; Houston, P. L. *J. Chem. Phys.* **1987**, *87*, 1445.
(27) Neumark, D. M.; Lykke, K. R.; Andersen, T.; Lineberger, W. C. *Phys. Rev. A* **1985**, *32*, 1890.
(28) Krems, R. V.; Buchachenko, A. A.; Szczesniak, M. M.; Klos, J.; Chalasinski, G. *J. Chem. Phys.* **2002**, *116*, 1457.
(29) Dunning, T. H. *J. Chem. Phys.* **1989**, *90*, 1007.
(30) Woon, D. E.; Dunning, T. H. *J. Chem. Phys.* **1993**, *98*, 1358.
(31) Woon, D. E.; Dunning, T. H. *J. Chem. Phys.* **1994**, *100*, 2975.
(32) Peterson, K. A.; Figgen, D.; Goll, E.; Stoll, H.; Dolg, M. *J. Chem. Phys.* **2003**, *119*, 11113.
(33) Cybulski, S. M.; Toczylowski, R. R. *J. Chem. Phys.* **1999**, *111*, 10520.
(34) Boys, S. F.; Bernardi, F. *Mol. Phys.* **1970**, *19*, 553.
(35) MOLPRO, version 2006.2, a package of ab initio programs, Werner, H.-J.; Knowles, P. J. ; Lindh, R.; Manby, F. R.; Schütz, M.; and others see http://www.molpro.net.
(36) Miller, T. M. *CRC Handbook of Chemistry and Physics*, 83rd ed.; CRC Press: Boca Raton, FL, 2002.
(37) Koutselos, A. D.; Mason, E. A.; Viehland, L. A. *J. Chem. Phys.* **1990**, *93*, 7125.
(38) Alpher, R. A.; White, D. R. *Phys. Fluids* **1959**, *2*, 153.
(39) Saha, H. P. *Phys. Rev. A* **1993**, *47*, 273.
(40) Medved, M.; Fowler, P. W.; Hutson, J. M. *Mol. Phys.* **2000**, *98*, 453.
(41) Canuto, S.; Castro, M. A.; Mukherjee, P. K. *Phys. Rev. A* **1994**, *49*, 3515.
(42) Ralchenko, Y.; Kramida, A. E.; Reader, J. and NIST ASD Team (2008). *NIST Atomic Spectra Database (version 3.1.5). [Online] Available*: http://physics.nist.gov/asd3 [2008, November 27]. National Institute of Standards and Technology, Gaithersburg, MD.
(43) Krems, R. V.; Buchachenko, A. A. *J. Phys. B: At. Mol. Opt. Phys.* **2000**, *33*, 4551.
(44) Berning, A.; Schweizer, M.; Werner, H. J.; Knowles, P. J.; Palmieri, P. *Mol. Phys.* **2000**, *98*, 1823.

JP903819M